Kinetically Enhanced Approach for Rapid and Tunable Self-Assembly of Rod–Coil Block Copolymers

Chun-Chih Ho,* Shang-Jung Wu, Shih-Hsiang Lin, Seth B. Darling, Wei-Fang Su*

A facile approach is reported to process rod–coil block copolymers (BCPs) into highly ordered nanostructures in a rapid, low-energy process. By introducing a selective plasticizer into the rod–coil BCPs during annealing, both the annealing temperature and time to achieve thermodynamic equilibrium and highly ordered structures can be decreased. This process improvement is attributed to enhanced chain mobility, reduced rod–rod interaction, and decreased rod–coil interaction from the additive. The novel method is based on kinetically facilitating thermodynamic equilibrium. The process requires no modification of polymer structure, indicating that a wide variety of desired polymer functionalities can be designed into BCPs for specific applications.

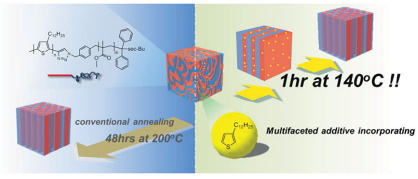

1. Introduction

Control of ordered nanostructures using rod–coil block copolymers (BCPs) has been recognized as a potentially valuable tool for biological[1] and optoelectronic[2–4] applications. Excitement surrounding these materials is rooted in their ability to concurrently self-assemble into a variety of hierarchical structures and their specific, tunable functionalities. In the past decade, through advances in polymer chemistry, rod–coil BCPs containing conjugated polymers have represented the majority of materials used in modeling studies of rod–coil BCPs,[5] in studies to establish experimental phase diagrams of rod–coil BCPs ,[6,7] and in optoelectronic applications.[2,8–12] In conventional coil–coil BCP systems, the Flory–Huggins interaction parameter (χ) and polymer volume fraction are dominant. Three additional parameters have emerged as dominant factors for determining the ultimate morphology of rod–coil BCPs: rod–rod interaction (μ, Maier–Saupe parameter),[13] competition between rod–rod interaction and rod–coil interaction ($G \equiv \mu/\chi$),[6] and aspect ratio from the rod block and coil block (ν).[14] A broad variety of nanostructures, such as irregular fibrils, alternating lamellae (LAM), hexagonally packed cylinders (HEX), bicontinuous gyroid (GYR), and body-centered-cubic array of spheres (BCC), have been observed.[14–16]

Poly(3-alkylthiophene) (P3AT)-based rod–coil BCP is of great interest due to potential applications in organic optoelectronics and transistors.[17] Nevertheless, this category of material usually self-assembles into randomly oriented nanofibril structures, bearing discontinuous character, which are not ideal for the performance of charge

Dr. C.-C. Ho, S.-J. Wu, Dr. S.-H. Lin, Dr. W.-F. Su
Department of Materials Science and Engineering
National Taiwan University
Taipei 106–17, Taiwan
E-mail: ccho76@ntu.edu.tw; suwf@ntu.edu.tw
Dr. C.-C. Ho, Dr. S. B. Darling
Center for Nanoscale Materials
Argonne National Laboratory
9700 South Cass Avenue, Lemont, IL 60439, USA
Dr. S. B. Darling
Institute for Molecular Engineering
University of Chicago
Chicago, IL 60637, USA

Macromol. Rapid Commun. **2015**, *36*, 1329–1335

DOI: 10.1002/marc.201500161

transport in the device. Aiming at ordered nanostructure rather than nanofibers for P3AT-based BCPs, few specific systems have been reported that meet the goal[18,19]; alternatively, one has to change the chemical structure of the polythiophene block. In our previous work,[14] to obtain versatile morphology, copolymers with stronger rod–coil interaction than rod–rod interaction were designed (i.e., the value of G should be small enough); otherwise, only lamellar structure will be obtained due to strong rod–rod interaction. We showed by altering rod–rod interaction, rod–coil interaction, and conformation asymmetry simultaneously, HEX and GYR phase could be observed near the symmetric composition of P3AT-based rod–coil BCPs.

In many cases, however, there are kinetic difficulties of strong segregation associated with obtaining ordered structure.[20] BCPs located in the strong segregation limit, say, $\chi N \approx 100$, usually suffer from retarded chain mobility. Due to confined diffusion pathways of polymer chains, trapped nonequilibrium structure persists even after thermal treatment is performed. Therefore, for two blocks with strong repulsive interaction (large χ), the BCP is limited to low molecular weight (small N) in order to reside sufficiently far away from the strong segregation limit, thereby restricting the choice of domain size; otherwise, extended thermal annealing at high temperature is required, which is time-consuming and energy-intensive. As an example, from our previous study,[14] the χ of poly(3-dodecyl thiophene)-*block*-poly(methyl methacrylate) (P3DDT-*b*-PMMA) rod–coil BCP was calculated to be 0.164 at 200 °C. The value is relatively larger than that of its analogue, polystyrene-*block*-poly(methyl methacrylate) (PS-*b*-PMMA) (0.0376 at 200 °C)[21] in the conventional coil–coil system. In order to reach thermodynamic equilibrium for nanostructure ordering, the copolymer has to be processed at high annealing temperature (200 °C) for long annealing time (2 d). Thus, researchers have intentionally suppressed rod–rod interaction and/or rod–coil interaction through modifying the chemical structures or reducing the degree of polymerization, which may deteriorate the performance in applications. To expand the applicability of rod–coil BCPs, it is vital to develop facile approaches to obtain highly ordered structures.

Blending polymers with copolymer is an extensively used technique,[22,23] particularly in conventional coil–coil BCP systems, to manipulate nanostructures with adjustable domain size and various morphologies without tedious synthetic effort. For instance, the "dry brush" concept has been developed, which involves introducing one or two corresponding homopolymers into a BCP and thus resulting in changeable domain size.[23] The selective additive concept has been established to tune structures by adding corresponding homopolymer with low molecular weight ("wet brush")[22] or small molecules[24] interacting with one or both blocks. Rod–coil BCP blends have also been studied through these blending approaches.[25–28] Whether the introduced homopolymer has a large molecular weight (should act as "dry brush") or small molecular weight (should act as "wet brush") in blends with copolymer, all results show only the domain size was changed in the lamellar structure, and unwanted macrophase separation occurred easily due to the low solubility of homopolymer in copolymer.[26,27,29] The origin of this phase separation is the large positive free energy of mixing from strong rod–rod interaction, strong rod–coil interaction, and low entropy mixing between the rod–coil BCP and the added homopolymer.[27]

Here, we have developed a unique strategy to overcome this challenge. By introducing a selective plasticizer into rod–coil BCPs, we easily manipulate and obtain the desired nanostructures. This additive possesses selective attraction to the rod block, the ability to temporarily enhance the chain mobility of the rod block, and lower rod–coil interaction between the molecules; ultimately, the additive can be removed from the copolymer matrix to restore its original functionality without deforming the formed nanostructures. Importantly, the method is free from chemical modification of the polymer structure, indicating a wide variety of desired polymer functionality could be designed and retained. P3DDT-*b*-PMMA was chosen as the model system of strong-segregated rod–coil copolymer. 3-Dodecylthiophene (3DDT) was selected as a selective plasticizer because it has similar chemical structure to the P3DDT block and encourages selective interaction, it is a liquid within the processing window to enhance the chain mobility of rod block, and it can be easily removed during thermal annealing.

2. Results and Discussion

Different compositions of P3DDT-*b*-PMMA were designed and synthesized to have various nanostructures. Two P3DDT-*b*-PMMAs, f_{PMMA} = 0.64 and 0.72, were prepared and denoted as **A** and **B,** respectively. Polymer characteristics are summarized in Table S1 (Supporting Information). All copolymers have narrow molecular weight dispersity ($Đ$) < 1.14, which ensures clear phase separation boundary from the self-assembly of copolymers. The detailed copolymer preparation is described in the experimental section and our previous work,[15] and the characterization data, including NMR spectra and gel permeation chromatography (GPC) traces, are placed in the Supporting Information.

In our previous work, we showed that P3DDT-*b*-PMMA has large χ = 0.164 even at high temperature.[14] Taking a sample without additive (**A-0** sample) as an example, we examined its morphological characteristics by temperature-dependent small-angle X-ray scattering (T-SAXS). The **A-0** sample was thermally annealed at 200 °C for 2 d.

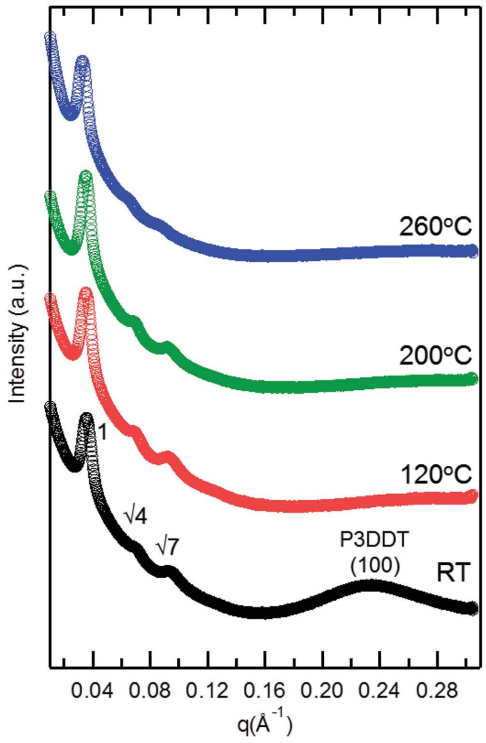

Figure 1. SAXS profiles of P3DDT-*b*-PMMA without additive (**A-0** sample) at different temperatures. Note that no order–disorder transition could be observed even at 260 °C.

Its SAXS profile (Figure 1) at room temperature shows a primary peak at q value of 0.041 Å^{-1} and high-order peaks in √4:√7 ratio, indicating hexagonally packed cylinders (HEX). The peak in the wide-angle region (q = 0.23 Å^{-1}) represents the crystallite peak of the P3DDT (100) plane. The copolymer is then heated with 5-min equilibria at each temperature. Upon heating above 90 °C, the peak of P3DDT (100) is diminished, indicating crystalline melting in the P3DDT block. With further heating, both scattered intensity and q value of the primary peak change little, suggesting the morphology is stable at such conditions. Even where the sample is heated up to 260 °C, the highly ordered peaks of HEX are still visible. Since there is thermal degradation of the PMMA block at high temperature, we did not prepare the sample above 260 °C to reach the disorder region and extract its χ value. Nevertheless, it is sufficient to deduce that the material has unusually high order–disorder transition temperature (T_{ODT}) and strongly segregated character. Hence, the material will suffer from poor kinetics, and it can serve as a good model for this study.

Figure 2a illustrates our proposed strategy to improve the self-assembly process of P3DDT-*b*-PMMA using monomer 3DDT additive. A 32 wt% of 3DDT was first blended with copolymer **A-0,** then dissolved in THF (good solvent for both blocks). The solvent was removed to make sample **A-32**, which would reduce the effective PMMA volume fraction (f'_{PMMA}) from 0.64 to 0.43, expected to change the morphology from hexagonally packed cylinders (HEX) to lamellae (LAM). It is intuitive that insufficient additive would not cause the proposed effect, and excess additive would simply destroy the self-assembled nanostructure. To identify an appropriate blending amount, we prepared samples containing different amount of 3DDT ranging from 0 to 65 wt% 3DDT. The detail data are shown in the Supporting Information. Consequently, we chose 32 wt% additive in copolymer (**A-32**) as a demonstration in the main text.

The nanostructures of **A-32** with different treatments were then investigated by SAXS measurement with calibrated absolute intensity as shown in Figure 2b. The SAXS profile of the as-cast sample **A-32** shows only one broad primary peak indicative of microphase separation in a poorly ordered state. As expected, the (100) peak around q = 0.23 Å^{-1} belonging to the P3DDT crystallite cannot be discerned since the 3DDT molecules work as a plasticizer and are selectively allocated within the P3DDT block of the copolymer. Thus, the growth of P3DDT crystallites is inhibited. The as-cast sample **A-32** was then annealed at 140 °C, which is 40 °C above the glass transition temperature of PMMA, for 1 h. Surprisingly, while f'_{PMMA} of the sample **A-32** is 0.43, meaning the morphology should be located in the lamellar phase, the SAXS profile (Figure 2b, red circles) shows a primary peak at q value of 0.041 Å^{-1} and significant multiple scattering peaks with the ratio of 1:√3:√4:√7:√9:√13, indicating that sample **A-32** was self-assembled into HEX structure. The (100) peak associated with the P3DDT crystallite appears with moderate intensity, suggesting a certain amount of 3DDT might evaporate during the annealing and thus shift f'_{PMMA} back into the HEX region. However, it is worth noting that the ordered HEX structure can be established with much lower annealing temperature (140 °C vs. 200 °C) and much shorter annealing time (1 h vs. 48 h) as compared to the sample **A-0**, and we will further discuss later.

To determine whether the morphology evolution could proceed further, the sample was annealed for 15 additional hours. The SAXS profile (Figure 2b, blue circles) still shows the HEX morphology but with changed intensities in the characteristic peaks and higher intensity of (100) peak from P3DDT crystallites. These results indicate that morphological evolution in the HEX phase occurred with the aid of 3DDT, and HEX phase remained after 3DDT removal; the P3DDT crystallite feature can be recovered through extended annealing to exhaust 3DDT almost completely. It is interesting to note that the sample with different annealing times of 1 h and 15 h shows identical primary peak q value, indicating the HEX structure has identical domain spacing in this annealing period. The sample for 1 h annealing has higher intensity in √3 and √9, and lower intensity in √7 than for 15 h

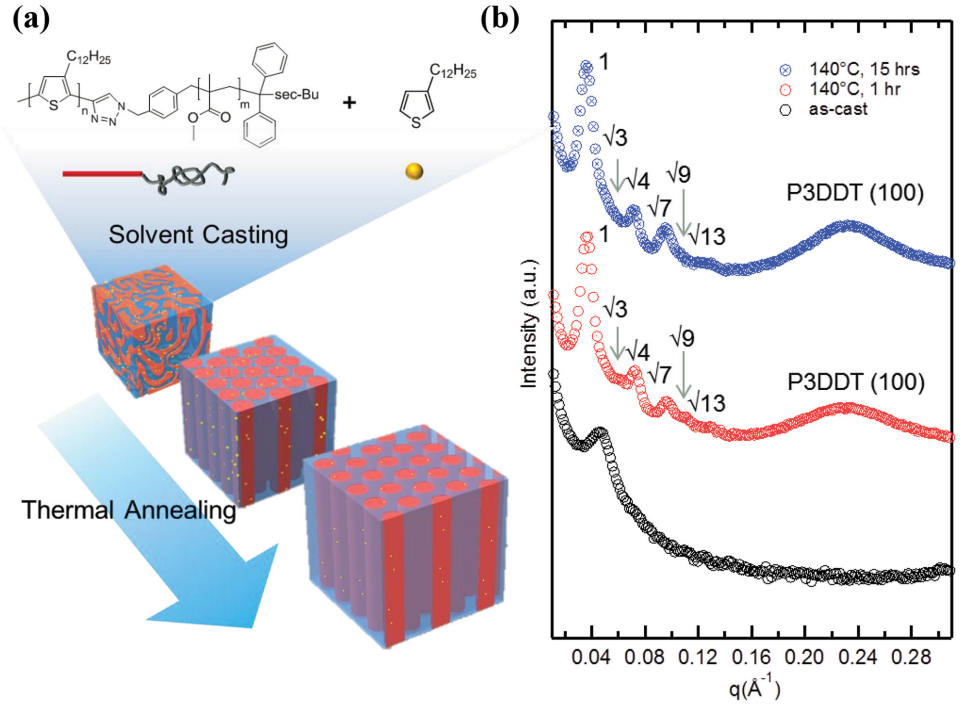

Figure 2. a) Schematic illustration of this unique blending strategy. b) SAXS profiles of **A-32** samples prepared in different conditions. Black, red, and blue circles represent samples as-cast, thermally annealed at 140 °C for an hour and for 15 h, respectively.

annealing, indicating the cylinder size in the sample following shorter annealing time is larger than that following longer annealing time. This phenomenon is illustrated in Figure 2a. To our best knowledge, this is the first demonstration of using a selective plasticizer acting as the internal solvent and the plasticizer filler incorporated within a thermal annealing procedure for achieving highly ordered nanostructure of BCP, although various strategies have been developed to reach and manipulate ordered structure in coil–coil BCP and rod–coil BCP systems.

To further verify the effectiveness of the selected additive and the structural evolution in detail, an in situ annealing experiment using SAXS was performed. The study can also reveal changes of morphology with time and volume fraction of polymer. From the discussion earlier, the sample **A-32** experienced extremely rapid relaxation at 140 °C. An annealing temperature at 120 °C, slightly higher than the T_g of PMMA, was used to reduce the chain relaxation rate of the polymer during the annealing procedure. The SAXS profiles were recorded at a 10-min increment during 600-min annealing time, and their corresponding curves are depicted in Figure 3a. In order to easily scrutinize these results for the investigation of morphology evolution, the intensity ratio of two characteristic peaks from two phases (√9 corresponds to the feature of LAM over √7 corresponds to the feature of HEX), the q value of primary peak (q^*) and the effective PMMA volume fraction (f'_{PMMA}) with time dependence are plotted in Figure 3b. The f'_{PMMA} and the weight fraction of the 3DDT (Figure S5, Supporting Information) were determined by thermogravimetric analysis (TGA) by assuming the weight loss only depends on the evaporation of additive (see the Supporting Information). Within 30 min, the SAXS curves show a primary peak with a growing peak of √9 in ratio, indicating symmetrical LAM structure is rapidly formed. The transmission electron microscopy (TEM) image (Figure 3c) shows the morphology of the sample annealed for 30 min is in the lamellar phase, but there are many defects and disordered regions, presumably because the morphology was formed and changed rapidly in this early annealing stage. These vigorous changes in morphology were also reflected in changes of the peak ratio, the q value of primary peak, and the PMMA volume fraction. After 1 h annealing, a new peak assigned to √4 appeared and grew with the peak at √9, indicating the morphology was still in the lamellar phase with asymmetric domain sizes. Figure 3d shows the TEM image of the sample annealed for 60 min. More regular lamellar structure and fewer defects are observed as compared to Figure 3c. While f'_{PMMA} was still gradually increasing and the changes of the peak ratio and the q value of the primary peak became slower in this stage, these nonequivalent changes and the highly ordered structure demonstrated from the results of SAXS and TEM suggest the morphologies were in a stable lamellar phase during this stage.

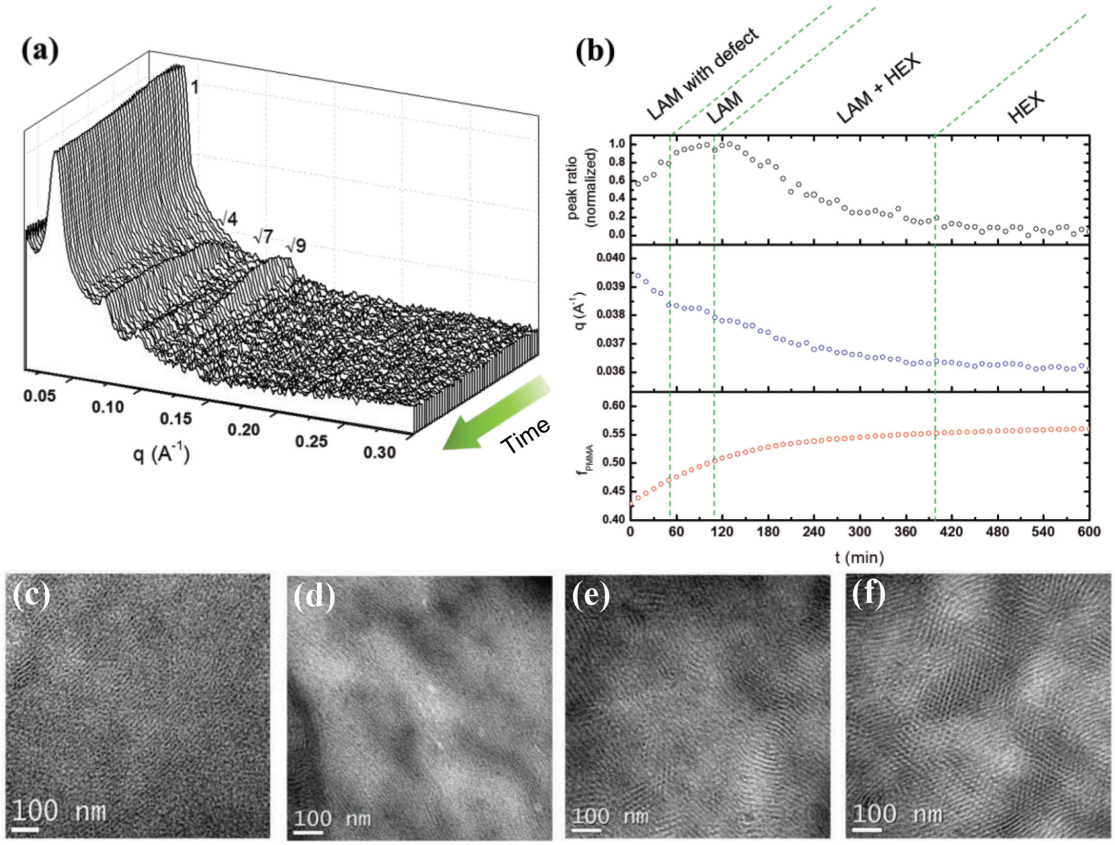

Figure 3. Study of in situ annealing by SAXS of **A-32**. a) The waterfall diagram of SAXS profiles depicts the morphological evolution from $t = 0$ to $t = 600$ min. Each curve is collected for 10 min. b) The intensity ratio of peak $\sqrt{9}$ to peak $\sqrt{7}$, the q value of primary peak, and effective volume fraction of PMMA are plotted together. TEM images of A-32 annealed for c) 30 min, d) 1 h, e) 4 h, and f) 10 h, respectively.

After 120 min of annealing, a new peak assigned to $\sqrt{7}$ in a ratio commenced to grow, the primary peak began to shift to lower q value, and the peak at $\sqrt{9}$ began to decline. While the effective volume fraction of PMMA was increasing, its pace of change became slower during the prolonged annealing time (>120 min); changes of the peak ratio and the q value of the primary peak became larger, indicating the sample might be going through an order-to-order transition of LAM-to-HEX. The TEM image (Figure 3d) of the sample annealed for 240 min provides a real-space indication of the morphological transition of LAM-to-HEX. In this micrograph, irregular cylindrical-like morphology and shorter lamellae (which could alternatively be interpreted to correspond to the lateral side of cylinders) are observed. As the annealing time extends beyond 420 min, all peaks of the SAXS profiles corresponding to HEX structure stop changing, and therefore the changes of peak ratio, q value, and f'_{PMMA} became diminished. The TEM image (Figure 3f) of the sample annealed for 600 min provides additional evidence that the morphology has completely converted into highly ordered HEX as compared to Figure 3e. This morphological transition of LAM-to-HEX was achieved after 400 min at 120 °C. The transition could originate from the fact that the relaxation rate of the copolymer was dramatically reduced due to evaporation of 3DDT additive (up to 80% was evaporated at this stage according to TGA data shown in the Supporting Information). Although the sample annealed at 120 °C takes a longer time to reach a stable morphology, the strategy still improved both the morphology and the annealing conditions as compared to previous work. Moreover, one can manipulate the desired structures (lamella or cylinder) with different time scales since the 3DDT additive is able to function as a plasticizer as demonstrated by SAXS and TEM results. Note, the f'_{PMMA} remained at 0.56 and did not completely shift back to 0.64 even after much longer annealing time (≈20 h). The results indicate that a strong interaction between the 3DDT additive and P3DDT block is likely present.

We further validate our approach is applicable for different compositions. The copolymer with higher volume fraction of PMMA ($f_{PMMA} = 0.72$), collectively denoted the **B** samples, was annealed at 200 °C for 48 h without the 3DDT additive and 140 °C for 21 h with the 3DDT additive. Interestingly, the morphological results (Figure 4) are quite different between these two samples. The SAXS

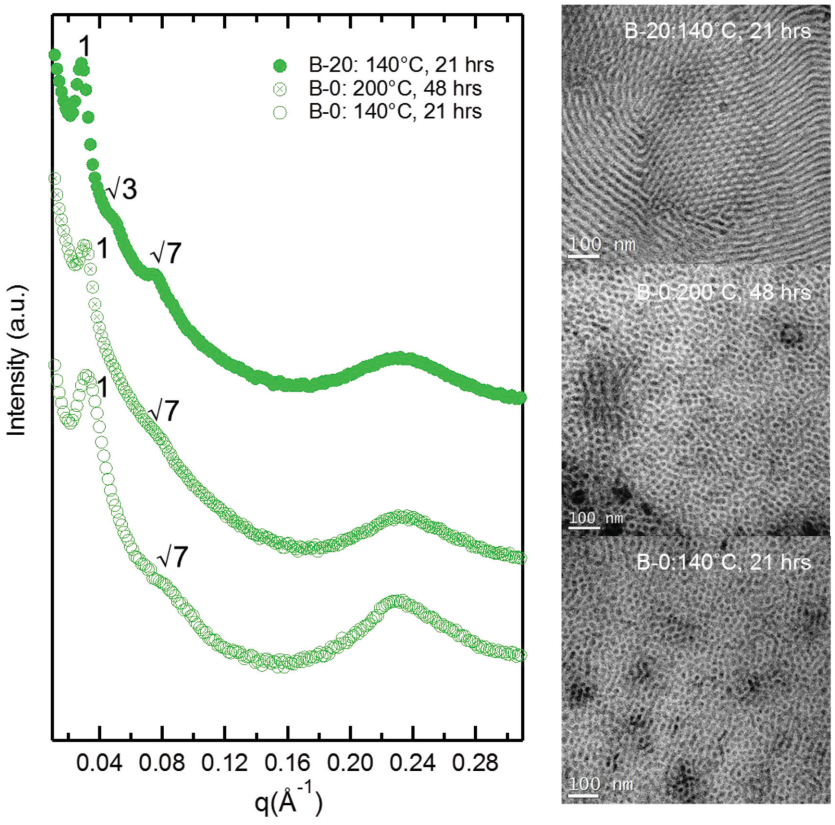

Figure 4. SAXS profiles and TEM images of **B-0** and **B-20** through different annealing conditions as indicated.

curve of **B-0** shows only one primary peak (q = 0.033 Å^{-1}) with a broad high order peak of √7, which might indicate the morphology is HEX structure or body-centered cubic spheres (BCC). The TEM image of **B-0** provides visual evidence showing solely irregular and circular structures can be observed, which suggests the morphology of sample **B** with 0.72 volume fraction is likely in the BCC phase. After the sample **B-20** was annealed with the incorporation of 3DDT, the primary peak was a bit shifted to 0.031 Å^{-1} and the intensity of the peak set increased with a new peak of √3 in ratio. This result indicates sample **B-20**, with the assistance of the additive, has better ordered structure as compared to sample **B-0**. However, the TEM image of sample **B-20** shows HEX structure and short lamellar structure, indicating the morphology is HEX phase rather than BCC phase. Since the **B-0** is also BCC structure at 140 °C (Shown in Figure 4), we confirm that the order-to-order transition is not purely originating from thermal induction. By adding 20 wt% of 3DDT into **B-0** to make **B-20**, the effective PMMA volume faction was changed from 0.72 to 0.62. Therefore, the HEX phase could be established in the very early stages of annealing procedure (as described in the paragraph of in situ measurements for sample **A**). Upon prolonged annealing, the 3DDT additive is rapidly evaporated and the B polymer chains might suffer from additional curvature mismatch originated from the entanglement of PMMA and/or recrystallization of the P3DDT chains.[30,31] Therefore, the B polymer would require more chain relaxation time than that of the **A** polymer to reorganize via the interface diffusion mechanism. As the results, the morphology of HEX phase could be retained.

3. Conclusion

In summary, we have successfully demonstrated a facile and effective means to form ordered structure rapidly and to control the desired nanoscale morphologies easily by introducing a selective plasticizer into rod–coil BCPs during annealing. A strong-segregated rod–coil BCP, P3DDT-*b*-PMMA, was used as a model system. With proper amount of 3DDT additive, morphologies with fewer defects and improved ordering in P3DDT-*b*-PMMA rod–coil BCP can be achieved at surprisingly low temperature with short annealing time. The promising results could be ascribed to the temporarily concurrent reduction of rod–rod interaction and rod–coil interaction. Furthermore, the in situ annealing experiment has shown that the selectivity of 3DDT enabled the copolymer to form lamellar phase initially, and an order-to-order transition (i.e., LAM-to-HEX) was observed as the 3DDT evaporated. The additive concept is also applicable to different BCP compositions. For instance, P3DDT-*b*-PMMA with higher PMMA volume fraction exhibits enhanced ordering using this approach. Instead of a BCC phase, fixed HEX phase was observed after thermal annealing, might attributed to the longer PMMA chain and the curvature mismatch caused by entanglement. The additive strategy establishes new insight into achieving ordered morphology easily in rod–coil BCP systems that will broaden their use in nanoscale applications.

Supporting Information

Supporting Information is available from the Wiley Online Library or from the author.

Acknowledgement: This research was financially supported by the Ministry of Science and Technology (104-3113-E-002–010 and 102-2221-E-002-230-MY3) and, in part, by the

US Department of Energy Office of Science, Program in Basic Energy Sciences, Materials Sciences and Engineering Division. The authors gratefully thank the Department of Chemistry and College of Bioresources and Agriculture of National Taiwan University for providing their NMR spectrometer and TEM microscope, respectively. Use of the Center for Nanoscale Materials at Argonne National Laboratory was supported by the US Department of Energy, Office of Science, Office of Basic Energy Sciences, under Contract No. DE-AC02–06CH11357.

Received: March 15, 2015; Revisde: April 20, 2015; Published online: May 21, 2015; DOI: 10.1002/marc.201500161

Keywords: additives; block copolymers; kinetics; rod–coil; self-assembly

[1] Y.-b. Lim, K.-S. Moon, M. Lee, *J. Mater. Chem.* **2008**, *18*, 2909.
[2] Y. F. Tao, B. McCulloch, S. Kim, R. A. Segalman, *Soft Matter* **2009**, *5*, 4219.
[3] S. B. Darling, *Energy Environ. Sci.* **2009**, *2*, 1266.
[4] I. Botiz, S. B. Darling, *Mater. Today* **2010**, *13*, 42.
[5] R. Holyst, M. Schick, *J. Chem. Phys.* **1992**, *96*, 730.
[6] C. C. Ho, Y. H. Lee, C. A. Dai, R. A. Segalman, W. F. Su, *Macromolecules* **2009**, *42*, 4208.
[7] B. D. Olsen, M. Shah, V. Ganesan, R. A. Segalman, *Macromolecules* **2008**, *41*, 6809.
[8] M. Shah, V. Ganesan, *Macromolecules* **2010**, *43*, 543.
[9] I. Botiz, S. B. Darling, *Macromolecules* **2009**, *42*, 8211.
[10] I. Botiz, A. B. F. Martinson, S. B. Darling, *Langmuir* **2010**, *26*, 8756.
[11] W.-C. Yen, Y.-H. Lee, J.-F. Lin, C.-A. Dai, U. S. Jeng, W.-F. Su, *Langmuir* **2010**, *27*, 109.
[12] M. Han, H. Kim, H. Seo, B. W. Ma, J. W. Park, *Adv. Mater.* **2012**, *24*, 6311.
[13] V. Pryamitsyn, V. Ganesan, *J. Chem. Phys.* **2004**, *120*, 5824.
[14] S.-H. Lin, S.-J. Wu, C.-C. Ho, W.-F. Su, *Macromolecules* **2013**, *46*, 2725.
[15] S. H. Lin, C. C. Ho, W. F. Su, *Soft Matter* **2012**, *8*, 4890.
[16] H. C. Moon, D. Bae, J. K. Kim, *Macromolecules* **2012**, *45*, 5201.
[17] B. Olsen, R. Segalman, *Mater. Sci. Eng. R: Rep.* **2008**, *62*, 37.
[18] C. A. Dai, W. C. Yen, Y. H. Lee, C. C. Ho, W. F. Su, *J. Am. Chem. Soc.* **2007**, *129*, 11036.
[19] R. H. Lohwasser, G. Gupta, P. Kohn, M. Sommer, A. S. Lang, T. Thurn-Albrecht, M. Thelakkat, *Macromolecules* **2013**, *46*, 4403.
[20] H. Yokoyama, *Mater. Sci. Eng. R: Rep.* **2006**, *53*, 199.
[21] S. Sakurai, K. Mori, A. Okawara, K. Kimishima, T. Hashimoto, *Macromolecules* **1992**, *25*, 2679.
[22] H. Tanaka, H. Hasegawa, T. Hashimoto, *Macromolecules* **1991**, *24*, 240.
[23] T. Hashimoto, H. Tanaka, H. Hasegawa, *Macromolecules* **1990**, *23*, 4378.
[24] K. J. Hanley, T. P. Lodge, C. I. Huang, *Macromolecules* **2000**, *33*, 5918.
[25] N. Sary, R. Mezzenga, C. Brochon, G. Hadziioannou, J. Ruokolainen, *Macromolecules* **2007**, *40*, 3277.
[26] Y. F. Tao, B. D. Olsen, V. Ganesan, R. A. Segalman, *Macromolecules* **2007**, *40*, 3320.
[27] C.-S. Lai, C.-C. Ho, H.-L. Chen, W.-F. Su, *Macromolecules* **2013**, *46*, 2249.
[28] L.-Y. Shi, I. F. Hsieh, Y. Zhou, X. Yu, H.-J. Tian, Y. Pan, X.-H. Fan, Z. Shen, *Macromolecules* **2012**, *45*, 9719.
[29] S. H. Ji, W. C. Zin, N. K. Oh, M. Lee, *Polymer* **1997**, *38*, 4377.
[30] M. Wang, A. Alexander-Katz, B. D. Olsen, *ACS Macro Lett.* **2012**, *1*, 676.
[31] M. Wang, K. Timachova, B. D. Olsen, *Macromolecules* **2013**, *46*, 5694.